



Cite this: *Phys. Chem. Chem. Phys.*,
2018, 20, 25482

Competition between hydrogen bonds and van der Waals forces in intermolecular structure formation of protonated branched-chain alcohol clusters†

Natsuko Sugawara,‡^a Po-Jen Hsu, iD ‡^b Asuka Fujii iD *^a and Jer-Lai Kuo iD *^b

To investigate the influence of bulky alkyl groups on hydrogen-bonded (H-bonded) network structures of alcohols, infrared (IR) spectra of protonated clusters of 2-propanol (2-PrOH) and *tert*-butyl alcohol (*t*-BuOH) were observed in the OH and CH stretch regions. In addition, by varying the tag species, the temperature dependence profile of the isomer population of $\text{H}^+(\text{i-BuOH})_n$ was revealed. An extensive search for stable isomers was performed using dispersion-corrected density functional theory methods, and temperature-dependent IR spectral simulations were done on the basis of the harmonic superposition approximation. The computational results qualitatively agreed with the observed size and temperature dependence of the H-bonded network structures of these protonated bulky alcohol clusters. However, the difficulty in the quantitative evaluation of dispersion was also demonstrated. It was shown that $\text{H}^+(2\text{-PrOH})_n$ ($n = 4\text{--}7$) have essentially the same network structures as the protonated normal alcohol clusters studied so far. On the other hand, $\text{H}^+(\text{i-BuOH})_n$ ($n = 4\text{--}8$) showed a clear preference for the smaller-membered ring structures, that is very different from the preference of the protonated normal alcohol clusters. The origin of the different structure preferences was discussed in terms of the steric effect and dispersion.

Received 16th August 2018,
Accepted 12th September 2018

DOI: 10.1039/c8cp05222k

rsc.li/pccp

I. Introduction

A hydrogen bond (H-bond) is a strongly directional intermolecular interaction because of the impact of its electrostatic interaction component.^{1,2} This directional character of the H-bond enables H-bonded systems to form clear network structures.³ H-bonded clusters in the gas phase are an ideal model system to explore such H-bonded network structures.

Clusters of alcohols, which have one proton donor (OH group) and two proton acceptor (lone pair) sites in each molecule, are one of the simplest models of H-bond networks.^{4–44} As a prototype of H-bonded clusters of alcohols, protonated

methanol clusters, $\text{H}^+(\text{MeOH})_n$, have been extensively studied by mass spectrometry, infrared (IR) spectroscopy, and theoretical calculations, and the dependence of their H-bonded network structures on cluster size and temperature has been well established.^{26–42} The H-bond network structures of protonated longer normal-chain alcohol clusters, $\text{H}^+(\text{n-alcohol})_n$, have also been investigated.^{32,42–44} For the protonated clusters of four *n*-alcohols (ethanol, 1-propanol, 1-butanol, and 1-pentanol), their structures at low and high temperatures (structures of the Ar tagged and bare clusters, respectively) have recently been determined in the size range of $n = 4\text{--}7$.⁴² At the low temperature (most stable structure), a competition between the linear and cyclic type structures, depending on the alkyl chain length, occurs at $n = 4$, while in the size range of $n = 5\text{--}7$, the structures of all the protonated *n*-alcohol clusters show essentially the same size dependence as that of $\text{H}^+(\text{MeOH})_n$. At the high temperature, all the clusters form linear chain structures at $n = 4\text{--}7$.

The magnitude of the van der Waals force, which includes both of attraction and repulsion, among alkyl chains should increase with increasing chain length. It has been actually suggested by the observed IR spectra of the protonated 1-butanol and 1-pentanol clusters that the interaction among these relatively long alkyl chains influences the H-bond strength in the clusters though their H-bonded network structures are the same as those

^a Department of Chemistry, Graduate School of Science, Tohoku University, Sendai 980-8578, Japan. E-mail: asuka.fujii.c5@tohoku.ac.jp

^b Institute of Atomic and Molecular Sciences, Academia Sinica, Taipei 10617, Taiwan. E-mail: jlkuo@pub.ams.sinica.edu.tw

† Electronic supplementary information (ESI) available: Temperature-dependent relative population of $\text{H}^+(\text{MeOH})_n$ ($n = 4\text{--}8$). Temperature-dependent relative population of $\text{H}^+(\text{2-PrOH})_4$. Temperature-dependent relative population of $\text{H}^+(\text{i-BuOH})_n$ ($n = 4\text{--}8$). Relative energies of structurally distinct isomers for $\text{H}^+(\text{MeOH})_4$, $\text{H}^+(\text{EtOH})_4$, $\text{H}^+(\text{2-PrOH})_4$, and $\text{H}^+(\text{i-BuOH})_4$. Simulated IR spectra of $\text{H}^+(\text{MeOH})_n$ ($n = 4\text{--}8$). Simulated IR spectra of $\text{H}^+(\text{2-PrOH})_4$. Simulated IR spectra of $\text{H}^+(\text{i-BuOH})_n$ ($n = 4\text{--}8$). The minimum free energy structures of $\text{H}^+(\text{2-PrOH})_4$ and $\text{H}^+(\text{i-BuOH})_n$ ($n = 4\text{--}8$). See DOI: 10.1039/c8cp05222k

‡ These authors contributed equally to this work.

of the protonated short-chain alcohols.⁴² This would be because the normal alkyl chain is highly flexible and its optimization of the conformation is possible without strong interference with the H-bond network. As a similar example in the gas phase, H-bond structures of neutral cyclohexanol clusters, $(\text{cyclohexanol})_n$ ($n = 3-6$), have been studied. It has been shown that these clusters form cyclic structures similar to those of neutral methanol clusters.^{45,46} This case demonstrates that the cyclohexyl group is flexible enough to avoid the strong interference with the optimized H-bond network. The same trend is seen also in crystalline structures of *n*-alcohols.⁴⁷⁻⁵³ The H-bond network structures in the crystals of ethanol, 1-butanol, and 1-pentanol are infinite linear (zigzag) chains, and they are essentially the same as that in crystalline methanol.

On the other hand, studies on bulky alcohols have elucidated a variety of crystalline structures, which are formed by the interplay between the H-bond and van der Waals force among bulky alkyl groups.⁵⁴⁻⁵⁷ As described above, crystals of *n*-alcohols are generally composed of H-bonded linear (zigzag) chains, and the van der Waals force among alkyl groups (mainly dispersion) binds these H-bonded chains. In contrast, alcohols with bulky alkyl groups tend to have cyclic or helical chain H-bond networks. For example, the H-bond structure of a 2-propanol crystal is a helical chain, and a *tert*-butyl alcohol crystal is composed of stacked four-membered H-bond rings.^{54,55} Such crystal studies demonstrate that rigid and bulky alkyl groups can be influential in H-bond network structures of alcohols. The interference between H-bonds and bulky alkyl groups has also been suggested by theoretical calculations of branched alkyl alcohols.⁵⁸

In the present study, we explore the influence of bulky alkyl groups on H-bond networks of protonated alcohol clusters. H-bonded network structures of protonated 2-propanol ($\text{H}^+(\text{2-PrOH})_n$, $n = 4-7$) and *tert*-butyl alcohol ($\text{H}^+(\text{t-BuOH})_n$, $n = 4-8$) clusters are studied by size-selective IR spectroscopy and theoretical calculations. IR spectra of the clusters are measured under two different temperature (internal energy) conditions, bare clusters produced in a supersonic jet expansion and Ar-tagged clusters. The cluster size range of $n = 4-7$ (up to 8 for *t*-BuOH) is examined. It has been demonstrated that $\text{H}^+(\text{MeOH})_n$ shows the H-bond network structure development from the simplest linear type to the most complicated “bicyclic” type in this size range.³⁵⁻⁴² The temperature dependence profile of the isomer population is explored in more detail for $\text{H}^+(\text{t-BuOH})_n$ by the variation of the tag species.^{41,42} Determination of the H-bond network structures of the protonated branched alcohol clusters is made through two stages. In the first stage, the observed spectra of the clusters are compared with those of $\text{H}^+(\text{MeOH})_n$, of which structures have already been well established, and the structures of the clusters are qualitatively determined on the basis of the spectral features. In the second stage, the observed spectra are compared with the results of density functional theory (DFT) calculations. Temperature dependence of the isomer populations and IR spectra are calculated under the harmonic superposition approximation (HSA). The qualitative assignments of the observed spectra are confirmed by the comparison with the HSA computation results.

II. Experimental

The $\text{H}^+(\text{2-PrOH})_n$ and $\text{H}^+(\text{t-BuOH})_n$ clusters and their Ar-tagged clusters were produced by electron ionization in a supersonic expansion. The sample vapor was mixed into the carrier gas (He/Ar 95:5 mixture), and was expanded to vacuum. A high pressure valve (Even-Lavie valve) was used for the jet expansion.⁵⁹ The stagnation pressure of the carrier gas was 7 MPa. The sample was put in the container that is located near the nozzle, and was heated at ~ 308 K. An electron beam accelerated to ~ -200 V from an e-gun (Omegatron Co.) was used for electron ionization. Both the bare and Ar-tagged clusters were formed under identical conditions, and they were mass-selected after their formation. To explore the internal energy (temperature) dependence of cluster structures, we also employed other tag species (Ne, N₂, CO₂, and acetylene). In the cases of N₂, CO₂, and acetylene, the tag sample (3–5%) is mixed with He gas. Neat Ne gas was used for Ne-tagging. The stagnation pressure of the carrier gas was 2 (CO₂- and acetylene-tagging) or 7 (Ne- and N₂-tagging) MPa.

IR spectra were measured by IR predissociation spectroscopy using a tandem quadrupole mass spectrometer with an octopole ion guide.⁶⁰ The IR light was the output of an optical parametric oscillator/amplifier (LaserVision) pumped by a Nd:YAG laser (Quanta-Ray, GCR-230). The spectra were recorded in the frequency range of 2800 to 3800 cm⁻¹. IR vibrational excitation induces the evaporation of alcohol molecule(s) or Ar tag atom(s). The fragment ion intensity was monitored as a measure of the IR absorption. For bare clusters, the loss channel of one alcohol molecule was monitored while the Ar loss channel was detected for the Ar-tagged clusters. Also in the case of the tagged clusters other than Ar, the tag loss channel was monitored.

III. Computation

Geometric optimization and Hessian analysis of protonated branched-chain alcohol clusters were performed using the Gaussian09 suite package at the B3LYP/6-31+G* (with and without the D3 correction) and ωB97XD/6-311+G(2d,p) levels of theory.⁶¹

To test the influence of various H-bond networks on simulated IR spectra, we started from the H-bonded structures of $\text{H}^+(\text{MeOH})_n$ compiled by Li *et al.* and transformed them into protonated branched-chain alcohol clusters.⁴⁰ The generation of the initial structures of $\text{H}^+(\text{t-BuOH})_n$ is straightforward; each of the three hydrogen atoms in the CH₃ group of methanol was substituted by a methyl group. In the case of $\text{H}^+(\text{2-PrOH})_n$, the substitution was carried out on two hydrogen atoms of CH₃, leading to 3^{*n*} possible configurations for each isomer of $\text{H}^+(\text{MeOH})_n$. In the database of $\text{H}^+(\text{MeOH})_n$, there are 2, 13, 22, 56, and 93 stable isomer structures for $n = 4, 5, 6, 7$, and 8, respectively. As a result, during the transformation, the number of $\text{H}^+(\text{2-PrOH})_n$ isomers grows rapidly, and it is beyond our computational capability (e.g., 162 isomers for $n = 4$, 3159 isomers for $n = 5$, 16 038 isomer for $n = 6$, and so on). As shown later, an essential difference between the observed spectra of $\text{H}^+(\text{2-PrOH})_n$ and $\text{H}^+(\text{MeOH})_n$ was found only at $n = 4$.

Therefore, we focused only on this size and performed its geometrical optimization and frequency calculation.

Besides the substitution process, one might need to consider the flexibility of the linear structure as well. In our previous work on the protonated ethanol cluster, $\text{H}^+(\text{EtOH})_4$, we have performed not only a side-chain permutation through the substitution but also a random conformer search for linear structures.⁴² This is because the energies of linear and cyclic structures were found to be very close after the optimization. Once the lowest energy structure is newly found in the conformation search, it would sensitively change the isomer population at low temperature. Nevertheless, our results of $\text{H}^+(\text{EtOH})_4$ showed that the extra linear conformers found in the additional search do not alter the conclusion regarding the relative stability of linear and cyclic structures.⁴² In the present work, we found that the cyclic structures of $\text{H}^+(2\text{-PrOH})_4$ are 0.5 to 2 kcal mol⁻¹ more stable than the linear ones when the initial structures were prepared only by the substitution process (see Fig. S4(g-i) in the ESI†), suggesting that additional conformer search for linear isomers should not affect the conclusion of the stability. Based on this reasonable notion, we did not perform additional search for linear conformers of $\text{H}^+(2\text{-PrOH})_4$.

Temperature dependency of the protonated branched-chain alcohol clusters was evaluated by the quantum harmonic superposition approximation (Q-HSA).^{62–64} Under this scheme, thermal contribution of each isomer to the IR spectrum is represented by

$$I_{\text{total}}(\omega, T) = \sum_a I_a(\omega) P_a(T),$$

where $P_a(T)$ is the canonical probability of the a th isomer which serves as a statistical population weight. The harmonic frequencies were scaled by a factor of 0.973 for B3LYP/6-31+G* and B3LYP/6-31+G*+D3, and 0.937 for ωB97X-D/6-311+G(2d,p). These scaling factors were determined to fit the free OH stretch bands of the experimental data. In addition, we applied a Lorentzian function to broaden the spectrum, in which the half-width at half-maximum values, γ , are 20 and 5 cm⁻¹ for free OH and CH stretch bands, respectively. As for H-bonded OH stretching modes, we adopted a power-law function of $\alpha(\Delta\omega)^\beta = \alpha(\omega_{\text{freeOH}} - \omega)^\beta$ for γ , which was proposed by Takahashi and co-workers for simulating the vibrational decay lifetime in the experiment, where $\Delta\omega$ is the red shift of the H-bonded OH band peak with respect to the free OH peak of the experimental spectra.^{65,66} The bandwidth of the H-bonded OH stretch was estimated by using the following parameterization: $\alpha = 0.0009$, $\beta = 1.9$, and $\omega_{\text{freeOH}} = 3678$ cm⁻¹, which was consistent with our previous works on the protonated methanol and water-methanol mixed clusters.^{39,40,67}

As shown in Section IV.A, through the analysis of the H-bond network topology, we identify four kinds of H-bond networks. All the possible isomers are categorized into one of these four types, and the categorization helps us to analyze H-bonded networks, their relative populations, and the temperature evolution of the IR spectrum. Our simulated Q-HSA results

and the comparisons with the observed spectra will be discussed in Section IV.D.

IV. Results and discussion

A. H-bond network structure types in protonated alcohols

Prior to introducing our results, we briefly review the topological properties of H-bonded network structures of protonated alcohol clusters.^{37–42} Possible network structures can be categorized into only four types, linear (**L**), cyclic (**C**), cyclic with a “tail” (**Ct**), and bicyclic (**bC**), which are schematically shown in Fig. 1. In all the types, the protonated site is highly acidic, and is always a double donor (DD) site in the observed size region. **L** has a one-dimensional chain-like structure, and is generally the most flexible structure type. The protonated site tends to locate at the center of the H-bond chain. Both the ends of the chain are single acceptor (A) sites and have a free OH. Sites between the protonated site and the end of the chain are single acceptor-single donor (AD) sites. When the two ends of an **L** structure are bound to each other by an H-bond, a **C** structure is formed. One of the terminal A sites becomes an AD site, and the other becomes a double acceptor (AA) site, which has a free OH. **Ct** is a structure in which a side chain (“tail”) is extended from the free OH of a **C** structure. This side chain is terminated by an A site. When the A site of a **Ct** structure is bound to the ring moiety, a **bC** structure is formed. It should be noted that no free OH exists in **bC**. Since all OHs are H-bonded, **bC** tends to be an energy favored structure when the construction of **bC** does not cause large strain.

The IR spectra of $\text{H}^+(\text{MeOH})_n$ in the OH and CH stretch regions were reported in our previous paper,⁴⁰ and they are reproduced in Fig. 2(a). Based on these spectra and the Q-HSA calculations, the H-bond network structures of $\text{H}^+(\text{MeOH})_n$ have been determined. The spectra of the bare clusters are reproduced well by the isomer population calculated at 200 K, and are attributed to the **L** structures at all the sizes. On the other hand, the spectra of the Ar-tagged clusters are reproduced

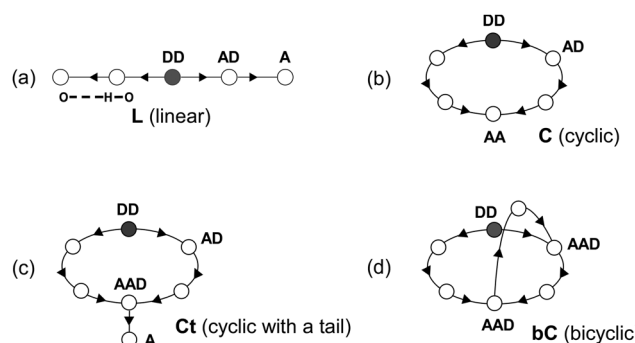


Fig. 1 Schematic representation of the four types of hydrogen bond network structures in protonated alcohols. An open circle represents an alcohol molecule, and an arrow indicates a hydrogen bond and its direction (from a donor to an acceptor). The protonated site, which is represented by a filled circle, plays the role of a double donor (DD) site. A, AA, AD, and AAD mean single acceptor, double acceptor, single acceptor-single donor, and double acceptor-single donor sites, respectively.

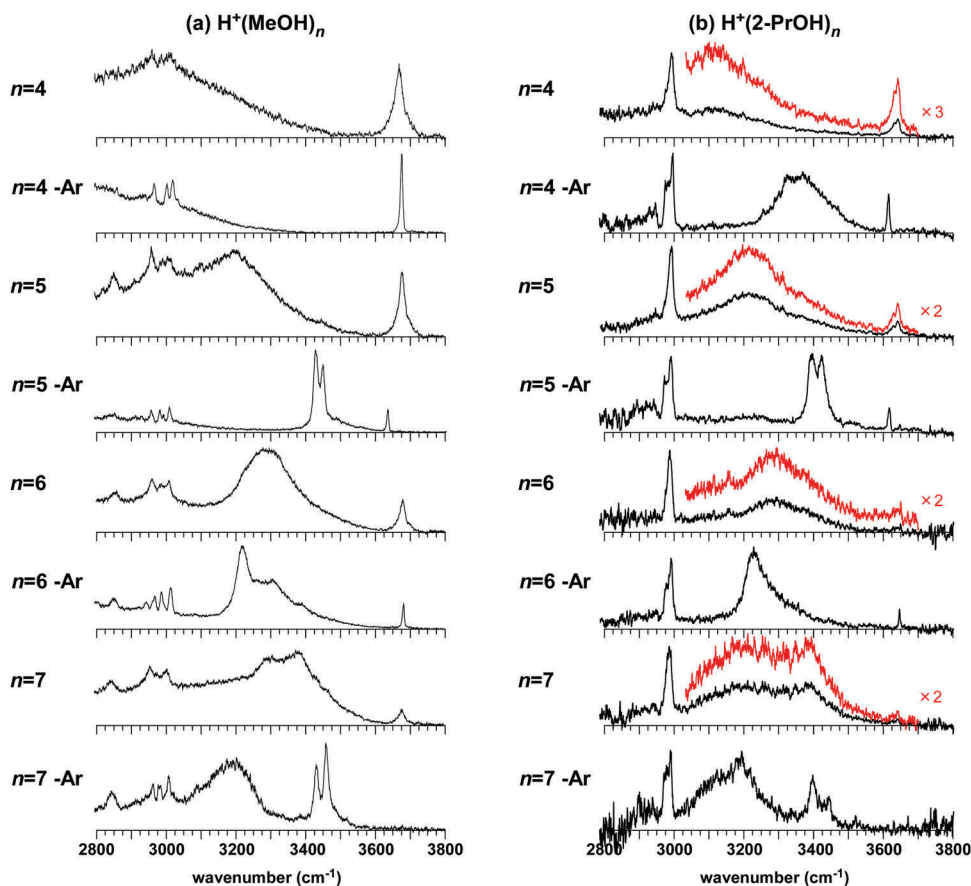


Fig. 2 IR spectra of (a) $\text{H}^+(\text{MeOH})_n$ and (b) $\text{H}^+(\text{2-PrOH})_n$ clusters in the OH and CH stretch regions. The scaled spectra in the OH stretch region (the red traces) of bare $\text{H}^+(\text{2-PrOH})_n$ are also presented for the convenience of comparison with the spectra of $\text{H}^+(\text{MeOH})_n$. The spectra of $\text{H}^+(\text{MeOH})_n$ are reproduced from ref. 40 with permission from the PCCP Owner Societies.

well by the simulation at 50 K, and the cluster structures are of the **L**, **C**, **Ct**, and **bC** types at $n = 4\text{--}7$, respectively. Each of these structures is the minimum energy one at its size. The spectra of $\text{H}^+(\text{MeOH})_n$ are used to discuss structures of $\text{H}^+(\text{2-PrOH})_n$ and $\text{H}^+(\text{t-BuOH})_n$, which are generated by the same ion source as $\text{H}^+(\text{MeOH})_n$.

B. Observed spectra and qualitative assignments of cluster structures

IR spectra of bare $\text{H}^+(\text{2-PrOH})_n$ and their Ar-tagged clusters are shown in Fig. 2(b). In those spectra, sharp free OH stretching bands appear in the 3600–3700 cm⁻¹ region, and the broad bands in the 2800–3600 cm⁻¹ region are attributed to H-bonded OH stretches. In addition, intense CH stretching bands are observed at ~ 3000 cm⁻¹. The spectral features of the bare and Ar-tagged clusters are very different from each other and this means that large structural changes occur upon Ar tagging.

First, we examine structures of the bare clusters of $\text{H}^+(\text{2-PrOH})_n$ on the basis of the observed spectra and comparison with those of $\text{H}^+(\text{MeOH})_n$. The CH stretching bands seem to be dominant in the spectra of $\text{H}^+(\text{2-PrOH})_n$ because of more CH oscillators in 2-PrOH than in MeOH. Since the spectra are normalized by the intensity of the CH stretching band, the OH stretch bands seem to be relatively suppressed. Therefore, the scaled spectra of the OH

stretch region (the red traces) are also displayed in the figure for the convenience of the comparison with $\text{H}^+(\text{MeOH})_n$. It is clearly seen that the spectral features of $\text{H}^+(\text{2-PrOH})_n$ are very similar to those of $\text{H}^+(\text{MeOH})_n$. This strongly suggests that bare $\text{H}^+(\text{2-PrOH})_n$ has the **L** structure at all the observed sizes. The frequency of the free OH stretching band (3640 cm⁻¹) is common for all bare $\text{H}^+(\text{2-PrOH})_n$, and it is lower than that of bare $\text{H}^+(\text{MeOH})_n$ (3674 cm⁻¹).

Next, we examine structures of Ar-tagged $\text{H}^+(\text{2-PrOH})_n$. In both the spectra of $n = 4$ and 5 of the Ar-tagged clusters, an intense band appears at around 3400 cm⁻¹, which is a marker band of the **C** structure (OH stretches H-bonded to the AA site).⁴⁰ Another evidence of the **C** structure is the frequency of the free OH stretch band. While the free OH in the **L** structure is in an A site, that of the **C** structure is in an AA site. It has been confirmed in $\text{H}^+(\text{MeOH})_n$ that the free OH frequencies of A and AA sites are different from each other, reflecting the difference between their H-bond coordination numbers.⁴⁰ In $\text{H}^+(\text{2-PrOH})_{4,5}\text{-Ar}$, their free OH frequency is shifted to low frequency by 30 cm⁻¹ from that of the bare clusters of the **L** structure. Because the spectrum of Ar-tagged $n = 6$ is very similar to that of $\text{H}^+(\text{MeOH})_6\text{-Ar}$ (and the spectral changes upon tagging are also parallel to the case of methanol), it is attributed to the **Ct** structure. The free OH frequency of the Ar-tagged cluster is the same as that of bare $n = 6$ of the **L** structure. This is also a

support of the **Ct** type structure since in both **L** and **Ct**, the free OHs are in A sites and they show the same frequency, as demonstrated in $\text{H}^+(\text{MeOH})_n$. The spectrum of Ar-tagged $n = 7$ is uniquely attributed to the **bC** structure because the free OH band is not observed.

Except for the case of $n = 4$, the observed structures of $\text{H}^+(\text{2-PrOH})_n$ are the same as those of $\text{H}^+(\text{MeOH})_n$ at the corresponding size. This means that a 1-methylethyl (isopropyl) group hardly interferes with the optimized H-bond networks of the clusters. It has been shown that the H-bond network in crystalline 2-PrOH is a helical chain with a three-fold axis while that in MeOH is a linear (zigzag) chain.^{47–50,54} The helicity of H-bonded chains cannot be recognized in the present analysis. If we exclude the helicity, both the networks are one-dimensional chains and are categorized into the same network type.

In Fig. 3, the IR spectra of $\text{H}^+(\text{t-BuOH})_n$ and $\text{H}^+(\text{t-BuOH})_n\text{-Ar}$ are shown in the size range of $n = 4\text{--}8$. The scaled spectra of the OH stretch region of the bare clusters are also displayed for convenience of comparison. Each spectrum of the bare clusters is quite similar to those of $\text{H}^+(\text{MeOH})_n$ and $\text{H}^+(\text{2-PrOH})_n$ at the corresponding size. This suggests that the bare $\text{H}^+(\text{t-BuOH})_n$ clusters at all the observed sizes have the **L** structure. On the other hand, the spectral features of Ar-tagged $\text{H}^+(\text{t-BuOH})_n$ seem to be very different from those of $\text{H}^+(\text{MeOH})_n$. In the following, we qualitatively examine the spectra of the Ar-tagged clusters to determine their H-bond network types.

At $n = 4$, the spectrum of the Ar-tagged cluster is very similar to that of $\text{H}^+(\text{2-PrOH})_4\text{-Ar}$. This spectrum clearly shows the marker band of the **C** type structure at *ca.* 3350 cm^{-1} , and the free OH band is shifted to low frequency from that of the **L** structure (bare cluster) by 30 cm^{-1} . A small band is seen at *ca.* 3700 cm^{-1} , and its frequency is too high for a free OH band. Therefore, this band is assigned to a combination band of the free OH stretch and an intermolecular vibration. $\text{H}^+(\text{MeOH})_4\text{-Ar}$ has the **L** structure, and a different preference for the H-bond network structure is found in 2-PrOH and *t*-BuOH at $n = 4$. In the protonated clusters of *n*-chain alcohols, it has been demonstrated that $\text{H}^+(\text{EtOH})_4\text{-Ar}$ also prefers the **C** structure while the Ar-tagged clusters of $\text{H}^+(\text{1-propanol})_4$, $\text{H}^+(\text{1-butyl alcohol})_4$, and $\text{H}^+(\text{1-pentanol})_4$ form the **L** structures.⁴² This competition between the **L** and **C** structures has been attributed to their extremely small energy difference and delicate contribution of dispersion at this size.

Upon the Ar tagging of $n = 5$, the peak position of the H-bonded OH band is not remarkably shifted. This contrasts with the case of $\text{H}^+(\text{MeOH})_5$ and $\text{H}^+(\text{2-PrOH})_5$; their Ar-tagged clusters clearly show the marker band of the **C** structure at around 3400 cm^{-1} . The lack of the marker band excludes the **C** structure for $\text{H}^+(\text{t-BuOH})_5\text{-Ar}$, and the appearance of a free OH band also denies the **bC** structure. Therefore, the **L** and **Ct** types, both of which show similar H-bonded OH stretch bands, are plausible candidates. Here, we note that the free OH band shows a small but definite shift to low frequency by *ca.* 10 cm^{-1} upon Ar-tagging. The magnitude of this shift is less than half of the shift upon the structural change from **L** to **C**, which is seen at $n = 4$. In the other protonated alcohol clusters (methanol,

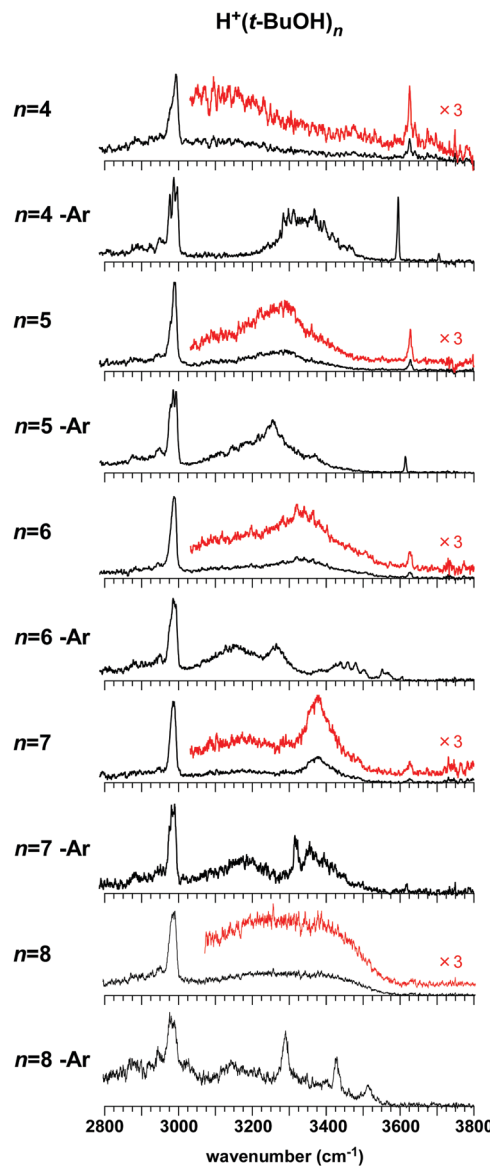


Fig. 3 IR spectra of $\text{H}^+(\text{t-BuOH})_n$ clusters in the OH and CH stretch regions. The scaled spectra in the OH stretch region (the red traces) are also presented for the bare clusters.

ethanol, 1-propanol, 1-butanol, 1-pentanol, and 2-propanol), the free OH stretch frequency of the **L** structure is exactly the same as that of the **Ct** structure because the free OH is in an A site in both structures.^{40,42} However, we assume that in the case of *t*-BuOH, this small shift is an indication of the structural change from **L** to **Ct** upon Ar-tagging. If the cluster holds the **L** structure upon Ar-tagging, the free OH shift upon tagging is attributed to the interaction between the Ar atom and the free OH group. This should result in a split of the two free OH bands in the **L** structure, but such a split is not seen in the observed spectrum. Therefore, it is more reasonable to attribute the shift to the structure change from **L** to **Ct**. The small shift to low frequency of the free OH band means the strength of the H-bond to the A site is enhanced in the **Ct** structure in comparison with that in the **L** structure. This structure assignment is confirmed by the computations, as shown later.

In the spectrum of the Ar-tagged $n = 6$ cluster, the free OH band is not observed. Therefore, **bC** type structures are dominant in the Ar-tagged cluster. However, a band is seen at $\sim 3580 \text{ cm}^{-1}$ in the spectrum. This band shows the existence of a very weak H-bond. When the side chain in a **Ct** structure is bound to the ring moiety, the H-bond network structure develops into a **bC** structure. When the actual structure is an intermediate between the **Ct** and **bC** structures, such a weak H-bond would occur at the bridge between the side chain and ring moiety. In the spectrum of $\text{H}^+(t\text{-BuOH})_7\text{-Ar}$, a free OH band is seen. Its frequency is different from those of the **L** (bare clusters) and **C** structures (tagged $n = 4$) but just agrees with that of the Ar-tagged $n = 5$ cluster. Therefore, **Ct** type structures are dominant in this cluster. In the spectrum of the tagged $n = 8$ cluster, the free OH band disappears. Therefore, its structure is uniquely determined to the **bC** type.

The observed low energy structures of $\text{H}^+(t\text{-BuOH})_n\text{-Ar}$ are totally different from those of $\text{H}^+(\text{MeOH})_n$ (and protonated n -chain alcohols) at the corresponding size. The H-bond network in crystalline *t*-BuOH is a cyclic structure composed of 4 molecules,⁵⁵ and this is very different from the linear (zigzag) chain in crystalline MeOH.^{47–50} We should note that the excess protons and the limited cluster size largely affect the H-bond structure. Moreover, some important factors in crystals, such as interactions among unit cells, are absent in the clusters. Therefore, the results on the clusters cannot be directly connected to the crystalline structures. However, it would be reasonable to conclude that the difference of the H-bond networks in the gas phase clusters reflects the different crystalline structures of alcohols.

C. Exploring temperature dependence profile of isomer population by the variation of tag species

The spectra of bare and Ar-tagged clusters inform us about the trend in structural changes of H-bond networks upon increasing the temperature. However, they correspond to measurements at two temperature points, and more detailed experimental confirmation on the temperature dependence profile of the isomer population is requested. For this purpose, IR spectra of $\text{H}^+(t\text{-BuOH})_{5,8}$ were observed with various tags other than Ar. It has been demonstrated that an increase of the binding energy with a tag allows survival of clusters with larger internal energy and this approximately corresponds to an increase in the temperature of these clusters.^{41,42}

Fig. 4 shows the observed IR spectra of $\text{H}^+(t\text{-BuOH})_5\text{-X}$ ($X = \text{Ne}, \text{Ar}, \text{N}_2, \text{CO}_2$, and acetylene (Ac)) with that of the bare clusters. The spectra of the bare and Ar-tagged clusters are reproduced from Fig. 3. From the bottom to the top of the figure, an increase in cluster temperature is expected with the increase of the magnitude of the interaction. The spectra of the Ne, Ar, and N_2 tags are essentially identical, and they are clearly attributed to the **Ct** structure, as described in the previous sections. With the CO_2 tag, three new bands appear at 3340, 3435, and 3580 cm^{-1} . The former two are assigned to the marker bands of the **C** structure (H-bonded OHs to the AA site), and the latter is its “free” OH bound to the CO_2 tag. The “free” OH in the **C** structure is shifted to low frequency

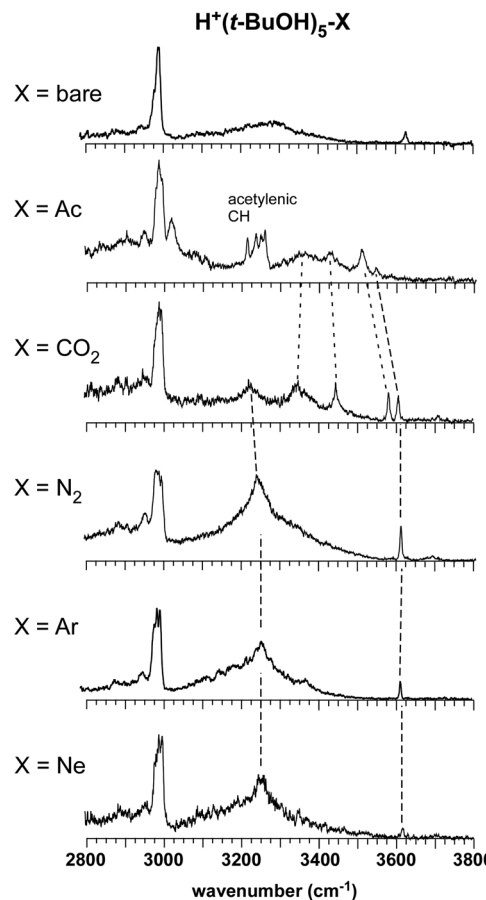


Fig. 4 IR spectra of $\text{H}^+(t\text{-BuOH})_5\text{-X}$ ($X = \text{Ne}, \text{Ar}, \text{N}_2, \text{CO}_2$, acetylene (Ac), and bare). The broken lines are eye guides to indicate the correlation among the bands.

by $\sim 20 \text{ cm}^{-1}$ from that of the **Ct** structure in $\text{H}^+(t\text{-BuOH})_n$. These observed features obviously demonstrated the coexistence of the **Ct** and **C** isomers in the CO_2 -tagged clusters. In the spectrum of the Ac-tagged cluster, the “free” OH stretch is further shifted by the π -H-bond formation with Ac, and the **C** isomer becomes dominant since one band is much stronger than the other in the “free” (or π -H-bonded) OH stretch region ($3500\text{--}3600 \text{ cm}^{-1}$). The bare cluster has **L** type structures, as shown in the above sections. Therefore, these spectral changes of the tagged clusters demonstrate the change of the dominant structure types from **Ct** to **C** and then to **L** with increase in temperature.

Similar measurements were also performed for $\text{H}^+(t\text{-BuOH})_8$. The IR spectra of the N_2 - and CO_2 -tagged clusters are shown in Fig. 5. The Ar-tagged cluster is uniquely found to have **bC** type structures. The spectrum of the N_2 -tagged cluster shows the coexistence of **bC** and another isomer which has a free OH. The latter can be attributed to the **Ct** isomer since the free OH frequency is higher than that of the **C** isomer. In the spectrum of the CO_2 -tagged clusters, the bands of the **bC** isomers disappear, and the spectrum is uniquely attributed to **Ct**. Therefore, the switch of the dominant isomer from **bC** to **Ct** and then to **L** upon increasing the temperature is shown.

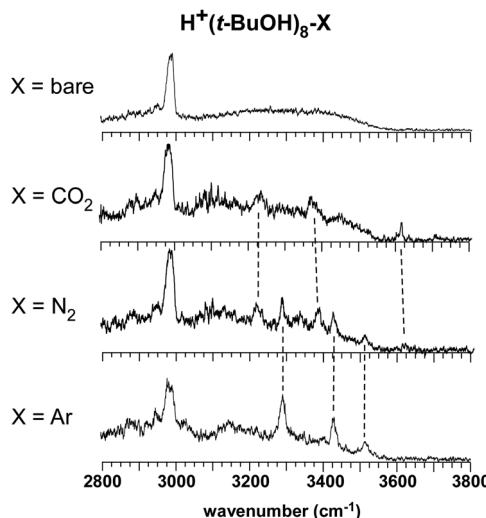


Fig. 5 IR spectra of $\text{H}^+(\text{t-BuOH})_8\text{-X}$ ($\text{X} = \text{Ar}, \text{N}_2, \text{CO}_2$, and bare). The broken lines are eye guides to indicate the correlation among the bands.

While the dominant isomer switch from the most stable one to the next stable one occurs with the CO_2 tag at $n = 5$, the switch at $n = 8$ is seen with the more weakly bound N_2 tag. This suggests that the dominant isomer switch occurs at lower temperature at $n = 8$ than at $n = 5$. These observations will be examined with the Q-HSA simulations in the next section.

D. Comparison with the Q-HSA simulations

We have examined the observed spectra on the basis of their features and qualitatively determined the cluster structures. Here, we compare the results of the above discussion with the theoretical isomer search and calculated temperature dependence of the isomer population. We first examined the Q-HSA results with B3LYP/6-31+G* (in the following, abbreviated as B3LYP). To further analyze the influence of the van der Waals force, we also performed calculations with the B3LYP/6-31+G*+D3 (B3LYP+D3) and ω B97X-D/6-311+G(2d,p) (ω B97X-D) levels of DFT and basis sets with dispersion correction. Our results show that the simulated IR spectra can qualitatively reflect the characteristics of the free OH stretching bands and the H-bonded vibrational modes in each H-bonded structure type (**L**, **C**, **Ct**, and **bC**). However, the agreement between the simulated temperature dependence and that of the observed spectra strongly depends on the level of theory. To systematically observe the trend of the functionals and the dispersion corrections, we made a complete scan on isomers of $\text{H}^+(\text{MeOH})_n$, $\text{H}^+(\text{2-PrOH})_4$, and $\text{H}^+(\text{t-BuOH})_n$ with these three levels of theory. We finally found that no single level of theory can reproduce all the size and temperature dependence of the observed spectra. Therefore, the best matched results to the observed spectra are picked up in this section. The theoretical temperature dependence of the isomer populations is summarized in Fig. 6. A comparison between the observed and simulated spectra is given in Fig. 7–10. The complete simulation results are summarized in the ESI† (Fig. S1–S15). Structures of the most populated isomer in each size and temperature are also displayed in the ESI† (Fig. S16–S20).

Starting from $n = 4$, our B3LYP calculations can qualitatively depict the observed spectra of the Ar-tagged and bare clusters (Fig. 7(a)–(c)). In $\text{H}^+(\text{MeOH})_4$, the simulated spectra predict the **L** structures at both 50 and 200 K.⁴⁰ On the other hand, in $\text{H}^+(\text{2-PrOH})_4$, the temperature-dependent population shows that with increase in temperature, the dominant H-bonded network changes from **C** (50 K) to **L** (200 K) (Fig. 6(a)), and the corresponding simulated spectrum also largely changes its features (Fig. 7(b)). This is in agreement with the observed change from the Ar-tagged (**C**) to the bare (**L**) clusters. The simulated spectrum at 50 K reveals the marker band of the **C** structure at around 3400 cm^{-1} (Fig. 7(b)). The double peak corresponds to the in-phase and out-of-phase OH stretches H-bonded to the AA site in the **C** structures. In the free OH stretch band, its frequency is blue shifted with the change from **C** to **L** by $\sim 21 \text{ cm}^{-1}$. This shift is 30 cm^{-1} in the observed spectra. Note that the CH stretch bands are always deviated from the observed one in the present simulations because we optimized the scaling factor only for the free OH stretch bands. In $\text{H}^+(\text{t-BuOH})_4$, the major isomer change from **C** to **L** at around 150 K is predicted with increase in temperature (Fig. 6(b)), and it supports the observed spectral changes from the Ar-tagged to the bare cluster. We also found that a characteristic band is predicted at 3300 cm^{-1} in the spectrum of the **L** structure at 400 K (Fig. 7(c), right panel). This band may be caused by the insufficient sampling of **L** structures since we consider only one **L** isomer in this simulated spectrum.

One can notice that both $\text{H}^+(\text{2-PrOH})_4$ and $\text{H}^+(\text{t-BuOH})_4$ have very similar spectral profiles. Both of them show the structural transition from **C** to **L** with increase in temperature. Nevertheless, according to Fig. 2 and 3, significant differences are found between $\text{H}^+(\text{2-PrOH})_n$ and $\text{H}^+(\text{t-BuOH})_n$ for $n > 4$. Our functional tests on $\text{H}^+(\text{t-BuOH})_n$ show that in spite of its success at $n = 4$, the B3LYP method totally fails in predicting reasonable temperature dependence at $n > 4$; the **L** structures are always dominant (Fig. S3(b–e) in ESI†). On the other hand, the ω B97X-D and B3LYP+D3 methods show qualitative agreement with the observed spectra of $n > 4$ (Fig. S3 in ESI†). The present results suggest that for the *tert*-butyl alcohol system, dispersion becomes more important with increasing cluster size, and even a qualitative discussion is difficult without the dispersion correction above the critical size of $n = 4$. However, the accuracy of both the ω B97X-D and B3LYP+D3 methods is still qualitative. Both of them do not succeed in reproducing the population change at $n = 4$. The simulated IR spectrum of $\text{H}^+(\text{t-BuOH})_4$ by B3LYP+D3 is presented in Fig. 7(d). The simulation shows that **C** should be observable even at 400 K. This clearly contradicts with the observed spectrum of the bare cluster, in which the marker band of **C** is totally absent (temperature of similar protonated clusters produced in the same ion source has been estimated to be around 150–200 K).^{39–42,67} Discrepancy between the ω B97X-D and B3LYP+D3 results is also seen in other sizes (Fig. S3 in ESI†). We found that within this size range the B3LYP+D3 method shows better agreement with the observed spectra than the ω B97X-D method.

To see the influence of the van der Waals force *versus* number of methyl groups, we examine the energies of $\text{H}^+(\text{MeOH})_4$,

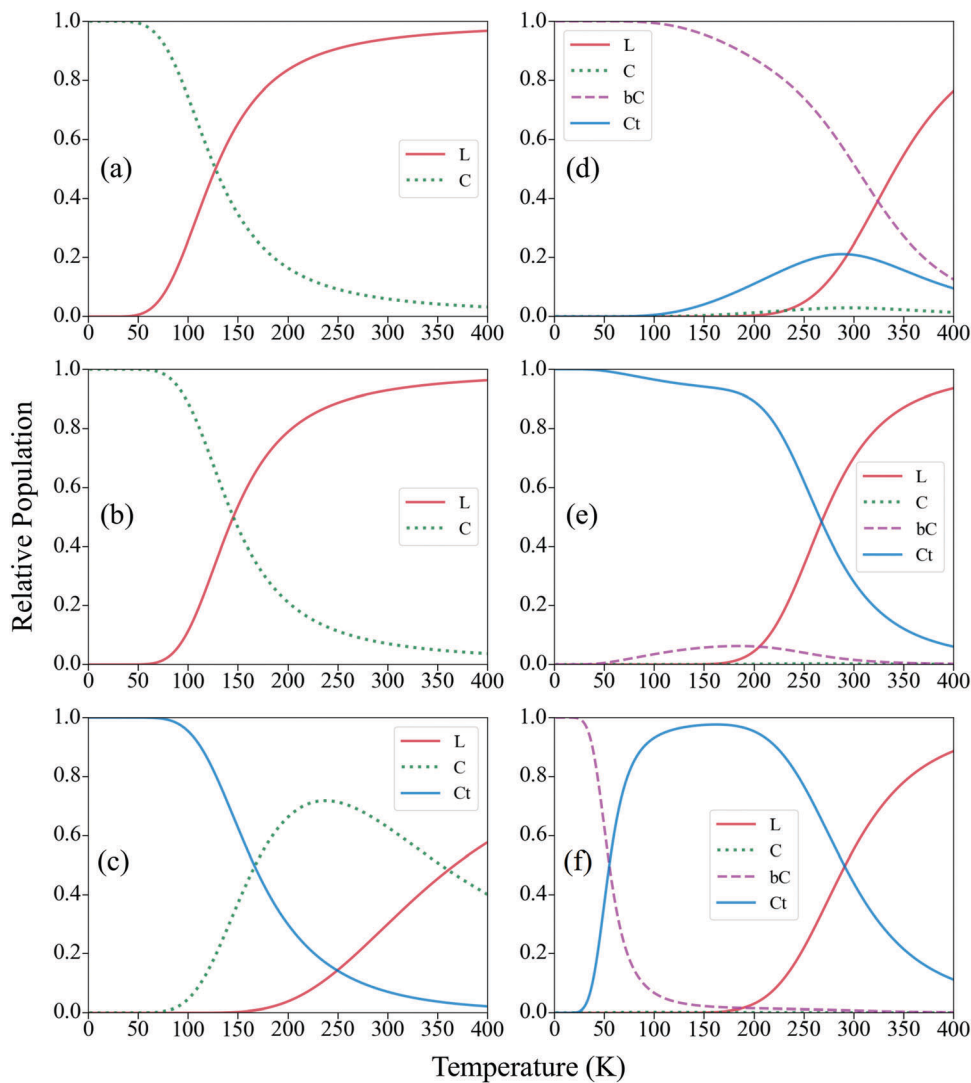


Fig. 6 Temperature dependence of the isomer population based on the Q-HSA calculations: (a) $\text{H}^+(\text{2-PrOH})_4$ -B3LYP, (b) $\text{H}^+(\text{t-BuOH})_4$ -B3LYP, (c) $\text{H}^+(\text{t-BuOH})_5$ -B3LYP+D3, (d) $\text{H}^+(\text{t-BuOH})_6$ -B3LYP+D3, (e) $\text{H}^+(\text{t-BuOH})_7$ -B3LYP+D3, and (f) $\text{H}^+(\text{t-BuOH})_8$ -B3LYP+D3. Isomer structures are categorized into the 4 types defined in Fig. 1, and are color-coded as follows; red for **L**, dotted green for **C**, dashed violet for **bC**, and blue for **Ct**. The relative populations are normalized.

$\text{H}^+(\text{EtOH})_4$, $\text{H}^+(\text{2-PrOH})_4$, and $\text{H}^+(\text{t-BuOH})_4$ in parallel. As shown in Fig. S4 in the ESI,[†] when the number of methyl groups is smaller and dispersion is less concerned, **L** is the most stable structure with a larger energy separation from **C**. As the number of methyl groups increases, **C** becomes more and more stable. Even B3LYP without the dispersion correction can catch this trend and this fact suggests that the transformation from **L** into **C** is at least partly driven by steric repulsion among the alkyl groups. With the dispersion correction, **C** becomes even more stabilized. In contrast, **L** becomes less and less favorable under larger dispersion and growing size effects. With this guideline, we can see the impact of these two effects on stabilizing the isomers, resulting in different thermal condition predictions.

It is also interesting to see how the simulated IR spectra depict the variation of tagging in $\text{H}^+(\text{t-BuOH})_5$ and $\text{H}^+(\text{t-BuOH})_8$ (Fig. 8). Again, we choose the simulated IR spectra by the

B3LYP+D3 method since they are the best matched results to the observed ones. In the variation of tagging of $\text{H}^+(\text{t-BuOH})_5$, the observed spectra can be well described by the simulated IR spectrum at 50 K (Ar-tagged), 150 K (CO_2 -tagged), and 400 K (bare). The corresponding major H-bonded structures are in good agreement with the observed spectra which suggest the dominance of **Ct** for the Ar-tagged, **Ct** and **C** for the CO_2 -tagged, and **L** for the bare clusters (Fig. 8(a)). In the case of **Ct** and **C** coexisting at 150 K, the free OH frequency of the **C** structure is 10 cm^{-1} lower than that of the **Ct** structure. In $\text{H}^+(\text{t-BuOH})_8$, the Ar-tagged spectrum shows no clear free OH band, suggesting the dominance of **bC**. The Ar-tagged spectrum can be depicted by the simulated IR spectrum at 50 K (Fig. 8(b), top figure). In fact, however, the Q-HSA population shows that **Ct** and **bC** co-exist at around this temperature (Fig. 6(f)) though the free OH band due to **Ct** is very weak. In the comparison of the

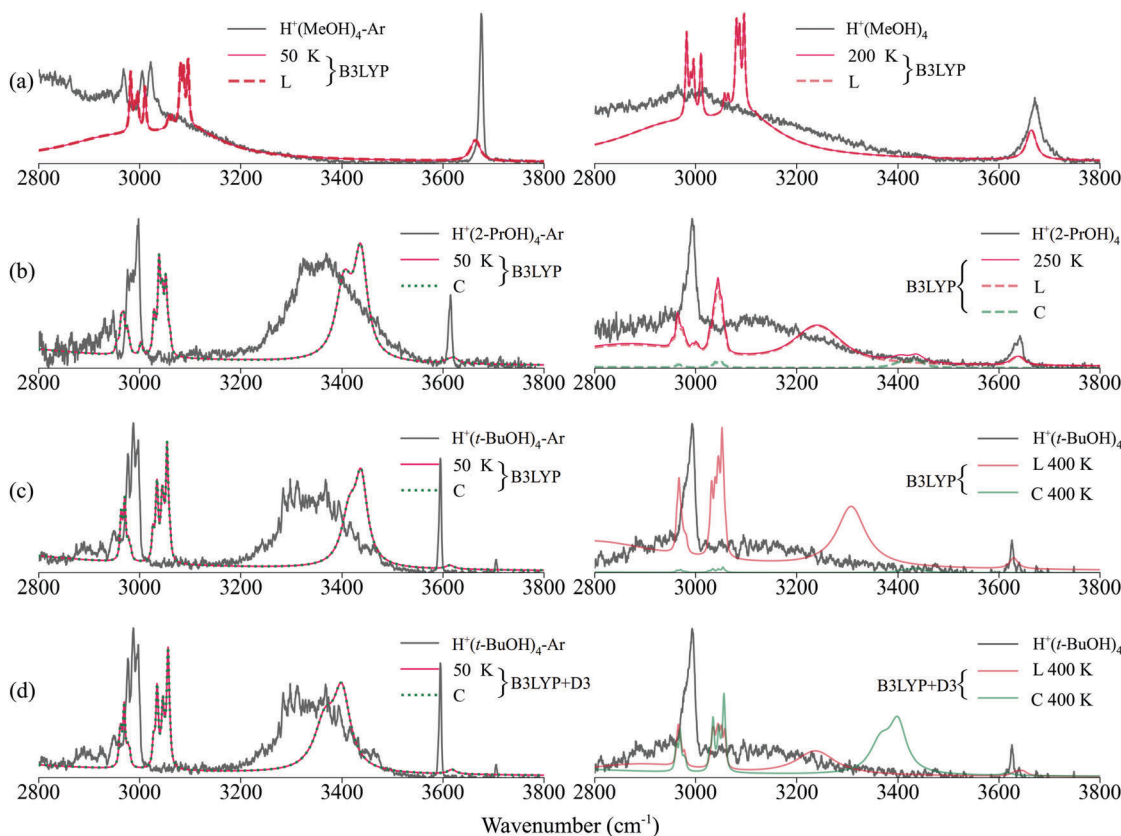


Fig. 7 Comparison between the observed IR spectra (black) of the Ar-tagged (left column) and bare (right column) clusters and the Q-HSA spectra for (a) $\text{H}^+(\text{MeOH})_4$ -B3LYP, (b) $\text{H}^+(\text{2-PrOH})_4$ -B3LYP, (c) $\text{H}^+(\text{t-BuOH})_4$ -B3LYP, and (d) $\text{H}^+(\text{t-BuOH})_4$ -B3LYP+D3. The Q-HSA spectra are represented by the total spectrum and/or single structure type spectra at each temperature, as shown in the legend.

CO_2 -tagged spectrum also with the 50 K spectrum, we zoomed in the frequency region around 3600 cm^{-1} and found a very weak free OH stretch band contributed by **Ct** (Fig. 8(b), middle figure). When temperature increases, **Ct** completely takes over **bC**. As for the bare clusters, a weak free OH stretching signal is attributed to **L**, which can be presented by the simulated IR spectrum at 400 K (Fig. 8(b), bottom figure). The observed trend of the major isomer switching with rise in temperature is well interpreted by the simulations. The switching temperature to **L** is, however, estimated to be about 400 K, and this temperature of the bare clusters seems to be too high, as we have pointed out in the case of $\text{H}^+(\text{t-BuOH})_4$. This error would be attributed to the overestimation of dispersion at this level of theory.

For $n = 5$ and 8, it is found that the B3LYP+D3 method is more reasonable than $\omega\text{B97X-D}$ in the prediction of the temperature dependence. This suggests the relative advantage of the D3 correction for the larger *tert*-butyl alcohol system ($n > 4$). Another evidence of this advantage is seen in the characteristic OH band at $\sim 3580 \text{ cm}^{-1}$ in the spectrum of Ar-tagged $\text{H}^+(\text{t-BuOH})_6$ (Fig. 9(a)). In the geometric optimizations by the three DFT methods we adopted in the present work, only B3LYP+D3 can successfully represent this band (Fig. S13 in ESI[†]). The most stable structure at the B3LYP+D3 level is **bC** as shown in Fig. 10. As seen in the comparison to the second most stable **bC** structure, the most stable structure is

actually an intermediate between **bC** and **Ct** structures. This structure has a very weakly H-bonded OH group, and its stretching band reproduces well the 3580 cm^{-1} band in the Ar-tagged spectrum. In contrast, the $\omega\text{B97X-D}$ method predicts a definite **Ct** structure as the most stable isomer. Hence, a clear free OH stretch band is seen at $\sim 3650 \text{ cm}^{-1}$ in the simulated spectrum at low temperature. This clearly contradicts the observed spectrum of the Ar-tagged cluster. Also for $n = 7$, the B3LYP+D3 method shows the best agreement with the observed spectra (Fig. 9(b)). The observed spectra of the Ar-tagged and bare clusters can be represented by the simulated IR spectra at 50 K and 300 K, respectively. The somewhat high temperature in the latter would be also attributed to the overestimation of dispersion.

Finally, we examine the free OH stretch frequency of the **Ct** structure in $\text{H}^+(\text{t-BuOH})_n$. In the qualitative analysis of the observed spectra of Ar-tagged $\text{H}^+(\text{t-BuOH})_n$, we assumed that the free OH frequency of the **Ct** structure is shifted to lower frequency by $\sim 10 \text{ cm}^{-1}$ than that of the **L** structure though both of them are in A sites. In the B3LYP+D3 simulations of $\text{H}^+(\text{t-BuOH})_n$, the free OH band in the **Ct** structure is shifted to low frequency by 5–8 cm^{-1} from that of the **L** structure. The $\omega\text{B97X-D}$ simulations also reproduce a similar trend of frequency shift in the **Ct** structure. These simulations well support the free OH frequency shift peculiar to the **Ct** structure

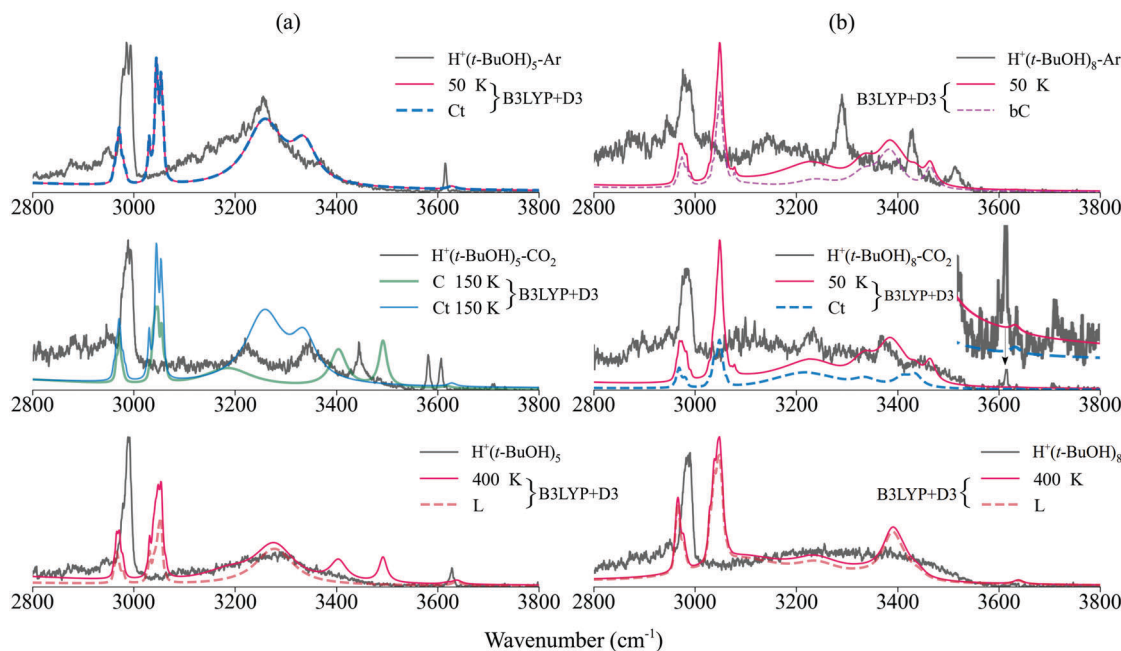


Fig. 8 Comparison between the observed IR spectra (black) of the Ar-tagged, CO₂-tagged, and bare clusters, and the Q-HSA spectra for (a) H⁺(t-BuOH)₅-B3LYP+D3 (left column) and (b) H⁺(t-BuOH)₈-B3LYP+D3 (right column). The Q-HSA spectra are represented by the total spectrum and/or single structure type spectra at each temperature, as shown in the legend. The total Q-HSA spectrum is not shown in the CO₂-tagged spectrum of H⁺(t-BuOH)₅.

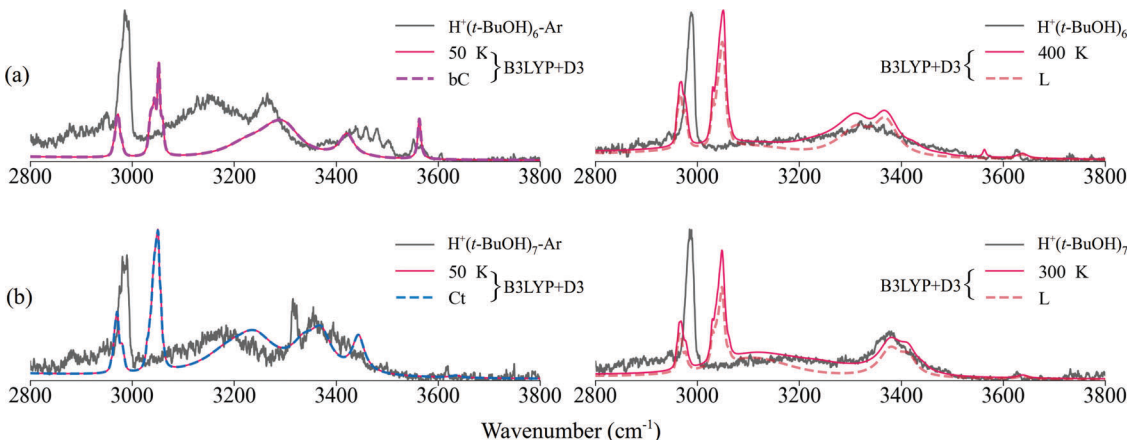


Fig. 9 Comparison between the observed IR spectra (black) of the Ar-tagged and bare clusters for (a) H⁺(t-BuOH)₆-B3LYP+D3 and (b) H⁺(t-BuOH)₇-B3LYP+D3. The Q-HSA spectra are represented by the total spectrum and/or single structure type spectra at each temperature, as shown in the legend.

of H⁺(t-BuOH)_n. This is also an example where characteristics of the observed IR spectra are reproduced well by the simulations though the evaluation of isomer energetics is more qualitative.

To sum up, the generic B3LYP method without the dispersion correction can well describe the branched alcohol clusters of size $n = 4$, including H⁺(MeOH)₄, H⁺(2-PrOH)₄, and H⁺(t-BuOH)₄. As for the H⁺(t-BuOH)_n clusters of $n > 4$, the dispersion correction is required to reproduce the observed structure trends. B3LYP with the D3 correction gives reasonable description of the observed spectra. Its crucial evidence is the weak H-bonded OH stretch band at around 3580 cm⁻¹ found in both the H⁺(t-BuOH)₆-Ar and the simulated IR spectrum at 50 K. Such a

band is absent in the simulations by both the B3LYP and ωB97X-D methods. However, the agreement between the B3LYP+D3 simulations and the observed spectral behaviors is still qualitative, and improvement of the dispersion correction is requested for a more quantitative discussion. In the H⁺(t-BuOH)_n system, $n = 4$ is a critical size. The bulky *tert*-butyl group causes both steric repulsion and attraction (dispersion). For sizes larger than $n = 4$, even a qualitative discussion is difficult without the dispersion correction. Also at $n = 4$, dispersion should play an important role in stabilizing the most stable C structure. The failure of the dispersion-corrected functionals at this size might arise from the overestimation of the magnitude of dispersion. The enthalpy

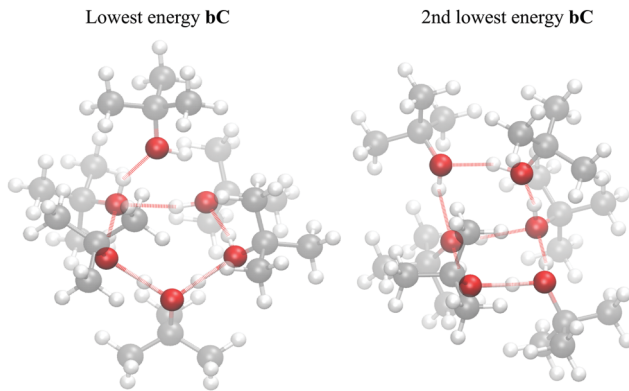


Fig. 10 The lowest (left) and the second (right) lowest energy isomers of $\text{H}^+(\text{t-BuOH})_6$ found by the optimization at the B3LYP/6-31+G*+D3 level. The former shows an intermediate structure between **bC** and **Ct**. The latter is a **bC** structure.

advantage of the **C** isomer over the **L** isomer is overestimated, and this makes the estimated isomer population switching temperature extraordinarily high (over 400 K, see Fig. S3 in ESI[†]). In other words, the success of B3LYP (without the dispersion correction) at this size might be also accidental. This is because B3LYP fails in reproducing the most stable structure of $\text{H}^+(\text{EtOH})_4$ while B3LYP-D3 succeeds in it.⁴² The balance between the **C** and **L** isomers in protonated alcohol tetramers is very delicate, and this is a good standard system to evaluate the precision of dispersion corrections.^{68–70} In the observation of this delicate balance between the **C** and **L** isomers, even a small difference in the binding energy with a tag can be a crucial factor. Though in the present theoretical analysis we assume that the role of tagging is only tuning the temperature of the cluster, the possibility of the isomer preference in tagging itself should be examined in future studies.

E. The origins of the H-bond network structure difference

With the Ar-tagging, the minimum energy structure at each size was experimentally explored and the results on $\text{H}^+(\text{t-BuOH})_n$ are well supported by the simulations. In $\text{H}^+(\text{t-BuOH})_n\text{-Ar}$, the observed structures are **C**, **Ct**, **bC**, **Ct**, and **bC** for $n = 4\text{--}8$, respectively. This H-bonded network development process with increasing size is very different from that in $\text{H}^+(\text{MeOH})_n$ (**L**, **C**, **Ct**, **bC**, and **bC** for $n = 4\text{--}8$, respectively),⁴⁰ while that of $\text{H}^+(\text{2-PrOH})_n$ is similar to $\text{H}^+(\text{MeOH})_n$ except for $n = 4$. In this section, we briefly discuss the origin of the structure difference among $\text{H}^+(\text{t-BuOH})_n$, $\text{H}^+(\text{2-PrOH})_n$ and $\text{H}^+(\text{MeOH})_n$.

The steric effect of the alkyl groups would be the most probable origin of the difference in the H-bond network structures. Bulky groups tend to be apart from each other, and such a trend generally results in the preference for smaller-membered ring (polygonal) structures since the external angle (of the polygon) is larger when the member of the ring is smaller. In the minimum energy structures of $\text{H}^+(\text{t-BuOH})_n$, such a preference for smaller-membered rings than those of $\text{H}^+(\text{MeOH})_n$ is clearly seen. As a general representation of the steric effect of alkyl groups, the *A*-value is frequently used.⁷¹

Table 1 Calculated binding energies of neutral homodimers. All units are in kcal mol⁻¹. The BSSE correction is involved. All binding energies are negative and the absolute values are taken in this table

	(MeOH) ₂	(2-PrOH) ₂	(<i>t</i> -BuOH) ₂
B3LYP/6-31+G*	5.18	4.83	4.69
B3LYP-D3/6-31+G*	6.50	7.55	8.19
ω B97X-D/6-311+G(2d,p)	5.73	7.44	7.04

The *A* value is defined by the relative Gibbs energy between the axial and equatorial conformations in substituted cyclohexane. The *A*-values of the methyl, 1-methylethyl (isopropyl), and *tert*-butyl groups are 1.7, 2.2, and 4.9 kcal mol⁻¹, respectively.^{72,73} The *A* values of the methyl and 1-methylethyl groups are similar to each other, while that of the *tert*-butyl group is much larger, indicating much more remarkable steric effect. These magnitudes of the *A* values correlate well with the difference of the H-bond network structure preferences among $\text{H}^+(\text{t-BuOH})_n$, $\text{H}^+(\text{2-PrOH})_n$ and $\text{H}^+(\text{MeOH})_n$. Here, we note that the bulky group also induces large dispersion. Therefore, not only repulsion but attraction also actually occurs among the bulky substituents and the balance between them should be considered, as described in the above sub-section.

Another factor we should examine is the H-bond strength because the alkyl group should affect both the acidity and basicity of alcohols. To simply evaluate the magnitude of the H-bond in these alcohols, we calculated the binding energies of their neutral homodimers. The calculated binding energies at the ω B97X-D/6-311+G(2d,p), B3LYP-D3/6-31+G*, and B3LYP/6-31+G* levels with the basis set superposition error (BSSE) correction are listed in Table 1. The binding energies at B3LYP are obviously underestimated by the lack of dispersion. The increase of the binding energy at ω B97X-D and B3LYP-D3 is more remarkable in 2-PrOH and *t*-BuOH, suggesting more contribution of dispersion to the binding energy with increasing size of the alkyl group. However, in both levels of theory, the binding energies of these three alcohols are more or less similar. The acidity of alcohol becomes lower with increase of the size of the alkyl group while the proton affinity increases. In the homodimer, these two effects almost cancel out each other. Therefore, the difference of the H-bond strength is not expected to be essential in the difference of the H-bond network structures. This is also supported by the observation that the peak positions of the H-bonded OH bands of the bare clusters, whose structures are commonly **L**, are very similar to each other among these three alcohols.

V. Conclusion

The H-bonded network structures of the protonated clusters of two branched alcohols were determined on the basis of IR spectroscopy and theoretical computations. The structures of $\text{H}^+(\text{2-PrOH})_{4\text{--}7}$ were quite similar to those of previously studied $\text{H}^+(\text{n-alcohol})_{4\text{--}7}$, and this suggests that the 1-methylethyl (isopropyl) group does not largely interfere with the energy-optimized H-bonded networks. In contrast, $\text{H}^+(\text{t-BuOH})_{4\text{--}8}$ tend to form small-membered cyclic structures. This trend is largely

different from the preference of the *n*-alcohols, because of the strong steric effect. The different structure trends of the two protonated branched-alcohol clusters would relate to the different crystalline structures of these alcohols. The Q-HSA simulations well supported the observed H-bonded structures. The dispersion correction to the density functionals was essentially needed to correctly reproduce the observed structure preference of $\text{H}^+(t\text{-BuOH})_n$. However, the agreement of the simulations with the observation was rather qualitative, indicating the limit of the present density functionals in quantitative evaluation of dispersion. With the variation of the tag species, the temperature dependence profile of the isomer population of $\text{H}^+(t\text{-BuOH})_n$ was revealed, and the results were consistent with the Q-HSA simulations.

Conflicts of interest

There are no conflicts to declare.

Acknowledgements

This study was partly supported by the Grant-in-Aid for Scientific Research (Project No. 18H01931) from JSPS. P. J. H and J. L. K. were supported by the Ministry of Science and Technology of Taiwan (MOST-107-2628-M-001-002-MY4) and Academia Sinica. Computational resources were supported in part by the National Center for High Performance Computing.

References

- 1 G. A. Jeffrey, *An Introduction to Hydrogen Bonding*, Oxford University Press, Oxford, 1997.
- 2 A. J. Stone, *The Theory of Intermolecular Forces*, Clarendon Press, Oxford, 1996.
- 3 J. Bernstein, R. E. Davis, L. Shimon and N.-L. Chang, *Angew. Chem., Int. Ed.*, 1995, **34**, 1555–1573.
- 4 U. Buck, J.-G. Siebers and R. J. Wheatley, *J. Chem. Phys.*, 1998, **108**, 20–32.
- 5 U. Buck and F. Huisken, *Chem. Rev.*, 2000, **100**, 3863–3890.
- 6 C. Steinbach, M. Fárník, I. Ettischer, J. Siebers and U. Buck, *Phys. Chem. Chem. Phys.*, 2006, **8**, 2752–2758.
- 7 R. N. Pribble, F. C. Hagemeister and T. S. Zwier, *J. Chem. Phys.*, 1997, **106**, 2145–2157.
- 8 F. C. Hagemeister, C. J. Gruenloh and T. S. Zwier, *J. Phys. Chem. A*, 1998, **102**, 82–94.
- 9 R. A. Provencal, R. N. Casaeas, K. Roth, J. B. Paul, C. N. Chapo, R. J. Saykally, G. S. Tschumper and H. F. Schaefer, III, *J. Phys. Chem. A*, 2000, **104**, 1423–1429.
- 10 A. K. Sum and S. I. Sandler, *J. Phys. Chem. A*, 2000, **104**, 1121–1129.
- 11 R. Ludwig, *ChemPhysChem*, 2005, **6**, 1369–1375.
- 12 R. Ludwig, *ChemPhysChem*, 2005, **6**, 1376–1380.
- 13 H. B. Fu, Y. J. Hu and E. R. Bernstein, *J. Chem. Phys.*, 2006, **124**, 024302.
- 14 S. Boyd and R. J. Boyd, *J. Chem. Theory Comput.*, 2007, **3**, 54–61.
- 15 R. W. Larsen, P. Zielke and M. A. Suhm, *J. Chem. Phys.*, 2007, **126**, 194307.
- 16 M. A. Suhm, *Adv. Chem. Phys.*, 2009, **142**, 1–57.
- 17 M. M. Pires and V. F. DeTuri, *J. Chem. Theory Comput.*, 2007, **3**, 1073–1082.
- 18 R. W. Larsen, P. Zielke and M. A. Suhm, *J. Chem. Phys.*, 2007, **126**, 194307.
- 19 H.-L. Han, C. Camacho, H. A. Witek and Y.-P. Lee, *J. Chem. Phys.*, 2011, **134**, 144309.
- 20 Y. Nishimura, Y.-P. Lee, S. Irle and H. A. Witek, *J. Chem. Phys.*, 2014, **141**, 094303.
- 21 T. Kobayashi, R. Shishido, K. Mizuse, A. Fujii and J.-L. Kuo, *Phys. Chem. Chem. Phys.*, 2013, **15**, 9523–9530.
- 22 R. M. Forck, C. C. Pradzynski, S. Wolff, M. Ončák, P. Slavíček and T. Zeuch, *Phys. Chem. Chem. Phys.*, 2012, **14**, 3004–3016.
- 23 M. Umer and K. Leonhard, *J. Phys. Chem. A*, 2013, **117**, 1569–1582.
- 24 S. Kazachenko, S. Bulusu and A. J. Thakkar, *J. Chem. Phys.*, 2013, **138**, 224303.
- 25 P. J. Hsu, K.-L. Ho, S.-H. Lin and J.-L. Kuo, *Phys. Chem. Chem. Phys.*, 2017, **19**, 544.
- 26 X. Zhang, X. Yang and A. W. Castleman Jr., *Chem. Phys. Lett.*, 1991, **185**, 298–302.
- 27 M. Meot-Ner, *J. Am. Chem. Soc.*, 1992, **114**, 3312–3322.
- 28 M. Meot-Ner, *Chem. Rev.*, 2012, **112**, PR22–PR103.
- 29 H.-C. Chang, J.-C. Jiang, S. H. Lin, Y. T. Lee and H.-C. Chang, *J. Phys. Chem. A*, 1999, **103**, 2941–2944.
- 30 H.-C. Chang, J.-C. Jiang, H.-C. Chang, L. R. Wang and Y. T. Lee, *Isr. J. Chem.*, 1999, **39**, 231–243.
- 31 Y. J. Hu, F. B. Fu and E. R. Bernstein, *J. Chem. Phys.*, 2006, **125**, 154306.
- 32 T. D. Fridgen, L. Macaleese, T. B. McMahon, J. Lemaire and P. Maitre, *Phys. Chem. Chem. Phys.*, 2006, **8**, 955–966.
- 33 K. Tono, J.-L. Kuo, M. Tada, K. Fukazawa, N. Fukushima, C. Kasai and K. Tsukiyama, *J. Chem. Phys.*, 2008, **129**, 084304.
- 34 E. S. Stoyanov, I. V. Stoyanova and C. A. Reed, *Chem. – Eur. J.*, 2008, **14**, 3596–3604.
- 35 J. J. Fifen, M. Nsangou, Z. Dhaouadi, O. Motapon and N.-E. Jaidane, *J. Chem. Theory Comput.*, 2013, **9**, 1173–1181.
- 36 J. J. Fifen, M. Nsangou, Z. Dhaouadi, O. Motapon and N.-E. Jaidane, *J. Chem. Phys.*, 2013, **138**, 184301.
- 37 A. Fujii, S. Enomoto, M. Miyazaki and N. Mikami, *J. Phys. Chem. A*, 2005, **109**, 138–141.
- 38 J.-L. Kuo, A. Fujii and N. Mikami, *J. Phys. Chem. A*, 2007, **111**, 9438–9445.
- 39 T. Hamashima, Y. C. Li, M. C. H. Wu, K. Mizuse, T. Kobayashi, A. Fujii and J.-L. Kuo, *J. Phys. Chem. A*, 2013, **117**, 101–107.
- 40 Y.-C. Li, T. Hamashima, R. Yamazaki, T. Kobayashi, Y. Suzuki, K. Mizuse, A. Fujii and J.-L. Kuo, *Phys. Chem. Chem. Phys.*, 2015, **17**, 22042–22053.
- 41 T. Shimamori, J.-L. Kuo and A. Fujii, *J. Phys. Chem. A*, 2016, **120**, 9203–9208.
- 42 A. Fujii, N. Sugawara, P.-J. Hsu, T. Shimamori, Y.-C. Li, T. Hamashima and J.-L. Kuo, *Phys. Chem. Chem. Phys.*, 2018, **20**, 14971–14991.

- 43 N. Solcà and O. Dopfer, *J. Am. Chem. Soc.*, 2004, **126**, 9520–9521.
- 44 N. Solcà and O. Dopfer, *J. Phys. Chem. A*, 2005, **109**, 6174–6186.
- 45 I. León, J. Millán, E. J. Cocinero, A. Lesarri and J. A. Ferández, *Angew. Chem., Int. Ed.*, 2013, **52**, 7772–7775.
- 46 I. León, R. Montero, A. Longarte and J. A. Ferández, *Phys. Chem. Chem. Phys.*, 2015, **17**, 2241–2245.
- 47 K. J. Tauer and W. N. Lipscomb, *Acta Crystallogr.*, 1952, **5**, 606–612.
- 48 B. H. Torrie, S.-X. Weng and B. M. Powell, *Mol. Phys.*, 1989, **67**, 575–581.
- 49 B. H. Torrie, O. S. Binbrek, M. Strauss and I. P. Swainson, *J. Solid State Chem.*, 2002, **166**, 415–420.
- 50 Ó. Gálvez, B. Maté, B. Martín-Llorente, V. J. Herrero and R. Escribano, *J. Phys. Chem. A*, 2009, **113**, 3321–3329.
- 51 P.-G. Jönsson, *Acta Crystallogr., Sect. B: Struct. Crystallogr. Cryst. Chem.*, 1976, **32**, 232–235.
- 52 P. Derollez, A. Hédoux, Y. Guinet, F. Danède and L. Paccou, *Acta Crystallogr., Sect. B: Struct. Sci., Cryst. Eng. Mater.*, 2013, **69**, 195–202.
- 53 M. Ramírez-Cardona, L. Ventolá, T. Calvet, M. A. Cuevas-Diarte, J. Rius, J. M. Amigó and M. M. Reventós, *Powder Diffr.*, 2005, **20**, 311–315.
- 54 S. A. Cirkel and R. Boese, *Acta Crystallogr., Sect. A: Found. Crystallogr.*, 2004, **60**, s205.
- 55 P. A. McGregor, D. R. Allan, S. Parsons and S. J. Clark, *Acta Crystallogr., Sect. B: Struct. Sci., Cryst. Eng. Mater.*, 2006, **62**, 599–605.
- 56 C. P. Brock and L. L. Duncan, *Chem. Mater.*, 1994, **6**, 1307–1312.
- 57 R. Tayler and C. F. Macrae, *Acta Crystallogr., Sect. B: Struct. Sci., Cryst. Eng. Mater.*, 2001, **57**, 815–827.
- 58 M. Huelsekopf and R. Ludwig, *J. Mol. Liq.*, 2002, **98–99**, 163–171.
- 59 U. Even, J. Jortner, D. Noy, N. Lavie and C. Cossart-Magos, *J. Chem. Phys.*, 2000, **112**, 8068–8071.
- 60 K. Mizuse and A. Fujii, *Phys. Chem. Chem. Phys.*, 2011, **13**, 7129.
- 61 M. J. Frisch, G. W. Trucks, H. B. Schlegel, G. E. Scuseria, M. A. Robb, J. R. Cheeseman, G. Scalmani, V. Barone, G. A. Petersson, H. Nakatsuji, X. Li, M. Caricato, A. Marenich, J. Bloino, B. G. Janesko, R. Gomperts, B. Mennucci, H. P. Hratchian, J. V. Ortiz, A. F. Izmaylov, J. L. Sonnenberg, D. Williams-Young, F. Ding, F. Lipparini, F. Egidi, J. Goings, B. Peng, A. Petrone, T. Henderson, D. Ranasinghe, V. G. Zakrzewski, J. Gao, N. Rega, G. Zheng, W. Liang, M. Hada, M. Ehara, K. Toyota, R. Fukuda, J. Hasegawa, M. Ishida, T. Nakajima, Y. Honda, O. Kitao, H. Nakai, T. Vreven, K. Throssell, J. J. A. Montgomery, J. E. Peralta, F. Ogliaro, M. Bearpark, J. J. Heyd, E. Brothers, K. N. Kudin, V. N. Staroverov, T. Keith, R. Kobayashi, J. Normand, K. Raghavachari, A. Rendell, J. C. Burant, S. S. Iyengar, J. Tomasi, M. Cossi, J. M. Millam, M. Klene, C. Adamo, R. Cammi, J. W. Ochterski, R. L. Martin, K. Morokuma, O. Farkas, J. B. Foresman and D. J. Fox, *Gaussian 09, Rev. E.01*, Gaussian Inc., Wallingford, CT, 2013.
- 62 D. J. Wales and I. J. Ohmine, *J. Chem. Phys.*, 1993, **98**, 7245–7256.
- 63 F. Calvo, J. P. K. Doye and D. J. Wales, *Chem. Phys. Lett.*, 2002, **366**, 176–183.
- 64 T. V. Bogdan, D. J. Wales and F. Calvo, *J. Chem. Phys.*, 2006, **124**, 1–13.
- 65 Y. L. Cheng, H. Y. Chen and K. Takahashi, *J. Phys. Chem. A*, 2011, **115**, 5641–5653.
- 66 M. Morita and K. Takahashi, *Phys. Chem. Chem. Phys.*, 2012, **14**, 2797–2808.
- 67 M. Katada, P.-J. Hsu, A. Fujii and J. L. Kuo, *J. Phys. Chem. A*, 2017, **121**, 5399–5413.
- 68 R. A. Mata and M. A. Suhm, *Angew. Chem., Int. Ed.*, 2017, **56**, 11011–11018.
- 69 A. Poblotzki, H. C. Gottschalk and M. A. Suhm, *J. Phys. Chem. Lett.*, 2017, **8**, 5656–5665.
- 70 S. Oswald and M. A. Suhm, *Angew. Chem., Int. Ed.*, 2017, **56**, 12672–12676.
- 71 E. L. Eliel and S. H. Wilen, *Stereochemistry of Organic Compounds*, John Wiley & Sons, New York, 1994.
- 72 H. Booth and J. R. Everett, *J. Chem. Soc., Perkin Trans. 2*, 1980, 255–259.
- 73 M. Manoharan and E. L. Eliel, *Tetrahedron Lett.*, 1984, **25**, 3267–3268.